doi: 10.82124/CEAS-GNC-2026-107 CEAS-GNC-2026-107

Super-Twisting Sliding Mode Control for Swing Reduction in UAV-Payload Systems

Sara Gomiero PhD student, Libera Università di Bolzano, Bolzano, Italy, and Politecnico di Bari, Bari, Italy. sara.gomiero@student.unibz.it, s.gomiero@phd.poliba.it

Spilios Theodoulis Associate Professor, Delft University of Technology, Delft, The Netherlands. s.theodoulis@tudelft.nl

Karl von Ellenrieder Full Professor, Libera Università di Bolzano, Bolzano, Italy. karl.vonellenrieder@unibz.it

ABSTRACT

This paper proposes Super-Twisting sliding mode controllers (STSMCs) to solve the trajectory tracking problem of a cargo Uncrewed Aerial Vehicle (UAV), while actively reducing the oscillations of the cable-suspended payload hanging from the quadrotor. In order to damp the oscillatory behavior of the cargo, we propose sliding surfaces which include the dynamics of the load swing angles. The proof of stability is carried out through Lyapunov analysis, resulting in finite-time convergence of the sliding surfaces and their derivatives, and asymptotic convergence of the tracking errors. Simulations in Matlab and Simulink are presented to show the effectiveness of the designed STSMCs, considering a small-scale cargo drone which performs a circular and a helical trajectory. Under the proposed controllers, the UAV is able to track the references, while the load swing angles do not exceed the magnitude of 2.5°. Our approach allows to reduce load oscillations by more than 50% when compared to STSMCs without active swing reduction.

Keywords: Uncrewed Aerial Vehicles, Suspended Payload, Sliding Mode Control, Swing Reduction

Nomenclature

x_E, y_E, z_E	=	North-East-Down (NED) reference frame axes
x_B, y_B, z_B	=	UAV body-fixed reference frame axes
x_{B_L}, y_{B_L}, z_{B_L}	=	Load body-fixed reference frame axes
ϕ, θ, ψ	=	Euler angles (roll, pitch, yaw)
x, y, z	=	UAV position (m)
α_L, β_L	=	Payload swing angles
F_x, F_y, F_z	=	Forces (N)
τ_ϕ, τ_θ, τ_ψ	=	Moments (N · m)
m_Q	=	UAV mass (kg)
m_L	=	Load mass (kg)
l	=	Cable length (m)
$I_{Q_{xx}}$, $I_{Q_{yy}}$, $I_{Q_{zz}}$	=	UAV diagonal inertia terms (kg · m^2)
I_{Lxx}, I_{Lyy}, I_{Lzz}	=	Load diagonal inertia terms (kg · m^2)

I_R	=	Propeller inertia (kg $\cdot$ m^2)
r_Q	=	Propeller radius (m)
r_L	=	Load radius (m)
c_T	=	Thrust coefficient N/(rad/s)^2
c_M	=	Torque coefficient N/(rad/s)^2
g	=	Acceleration of gravity (m/s^2)
ω_i	=	Rotational speed of i-th propeller (RPM)

1 Introduction

The control of quadrotor Uncrewed Aerial Vehicles (UAVs) with cable-suspended payloads poses several challenges, due to the underactuation, coupling, and nonlinearities of such systems. During transportation tasks, the UAV translational dynamics are strongly affected by the load, which undergoes oscillations. These vibrations are divided into transient and residual ones, where the former present a risk to both the UAV and the payload, while the latter augment the time required to accurately place the load at the final delivery point [1]. The swinging behavior must be counteracted or suppressed to avoid performance degradation, instability, and damage. The stabilization problem that arises is analogous to that of an inverted pendulum or a payload suspended from an overhead crane [2], [3], and it is particularly challenging due to the absence of direct control input on the load [4].

Inspired by solutions developed for cranes, researchers have designed different anti-swing control strategies for cargo drones, aiming to dampen excessive payload oscillations [5]. Such techniques either (1) generate swing-free feasible trajectories, closing the control loop on the load, or (2) counteract the load swing. In case (1), many works employ dynamic programming and reinforcement learning to optimize swing-free trajectories [4], however resulting in expensive computations. In case (2), to minimize the swinging behavior, both feedforward and feedback solutions have been proposed.

One of the most common and effective open-loop methods is input shaping, in which vibrations are reduced by taking the convolution of an impulse sequence with the desired input command. For example, the authors in [6] implement a nonlinear model-based controller with input shaping for a cargo drone, estimating the natural frequency of the system and the damping ratio, and subsequently evaluating the amplitude and the time locations of the impulses.

In contrast, feedback control strategies reduce the payload oscillations by exploiting the measurement and/or the estimation of the states [6]. Among such strategies, Interconnection and Damping Assignment-Passivity Based Control (IDA-PBC) is suggested in [7], due to its robustness against parametric uncertainty and unmodeled dynamics. Considering point to point motion in the planar case, two control laws are derived - one incorporating the swing angles, and the other independent of them.

Alternatively, first order sliding mode control (SMC) techniques are employed in [1] and [8] to diminish load oscillations. Furthermore, non-singular terminal SMC and Super-Twisting SMC laws are designed in [9] for UAV rotational and translational control, together with a nonlinear anti-swing controller, which ensures exponential convergence of the load swing motion. Instead, adaptive SMC solutions are developed in [10] to estimate and minimize the load vibrations by considering the oscillations of the suspended cargo as unknown and external disturbances. Similarly, [11] handles the swing angles of the uncertain suspended load as external disturbances, consisting of known components and bounded uncertainties. The former are compensated in the SMC law, while the latter are estimated via a sliding mode disturbance observer.

Different modeling and approach techniques are proposed in [12], where the flexible cable is treated as a series of connected links, and a geometric controller is derived to asymptotically stabilize the UAV position, while vertically aligning the cable below it and driving the swing angles to zero. However, this

approach may be challenging to be implemented without supplementary sensors for the evaluation of the state of each link.

In this work we use the Lagrangian formulation to model both the aerial vehicle and the cable-suspended load as rigid bodies. Assuming small swing angles, the UAV translational dynamics and the load swing angles dynamics are simplified for control purposes, resulting in decoupled equations. Inspired by the works of [13] and [14] on 3D overhead cranes, we propose Super-Twisting sliding mode (STSM) controllers to solve the trajectory tracking problem and attenuate oscillations of the cargo. We specifically design sliding surfaces for the translational control, including both the UAV trajectory tracking errors and the swing angles. Via Lyapunov theory, the stability of the sliding mode dynamics is investigated locally. Differently from [1], the derivation of the controllers is carried out in three dimensions and the chattering phenomenon is attenuated through second order sliding mode techniques. The proposed control strategy requires full state information of the cargo drone, including the UAV position and orientation as well as the load swing angles, which are typically obtained in indoor environments using motion capture systems. In contrast to neural network–based approaches, our method involves tuning only a limited number of parameters. Nevertheless, the tracking performance and disturbance attenuation capabilities of the STSM controllers depend on the assumed bounds of external disturbances. Consequently, the sliding surface coefficients may require retuning when the system operates under different disturbance conditions. Furthermore, it should be emphasized that performance may degrade during aggressive maneuvers, where the small-angle assumption is violated.

The rest of the paper is organized as follows. Section 2 is devoted to the derivation of the equations of motion of the UAV-payload system. Section 3 presents the design and the stability analysis of the Super-Twisting sliding mode controllers with swing reduction. Simulations are shown and discussed in Section 4. To conclude, Section 5 summarizes the work and provides insights about future directions.

2 Modeling of the UAV-payload system

The UAV-payload system studied in this paper is depicted in Fig. 1.

The system can be described through the vector of generalized coordinates $\boldsymbol{q} := [\boldsymbol{\xi}, \boldsymbol{\eta}, \boldsymbol{\mu}]^T \in \mathbb{R}^3 \times \mathbb{S}^3 \times \mathbb{S}^2$, defined in the NED frame, where $\boldsymbol{\xi} = [x, y, z]^T$, $\boldsymbol{\eta} = [\phi, \theta, \psi]^T$, and $\boldsymbol{\mu} = [\alpha_L, \beta_L]^T$. To simplify the derivation of the equations of motion, the following assumptions are made.

Assumption 1 (from [16]) *We assume that:*

1) *The structure of the quadrotor is rigid, symmetrical and cross-shaped.*
2) *The payload is a rigid body.*
3) *The cable is rigid, massless and always taut during the transportation task.*
4) *The origin of the body-fixed frame of the UAV coincides with its center of mass.*
5) *The distance between the center of mass of the UAV and the suspension point is short, compared to the length of the cable.*
6) *Non-aggressive maneuvers are performed. This implies that the roll, pitch and swing angles are within $(-\pi/2, \pi/2)$, while the yaw angle operates in $(-\pi, \pi)$.*

Remark 1 *Assumption 1 is generally valid when considering commercial vehicles executing transportation tasks with boxes. Indeed, it is reasonable to assume that the quadrotor performs non-aggressive maneuvers to avoid unsafe operations. In such scenarios, the cable can be considered to be rigid and taut [17], and its mass is usually negligible with respect to those of the UAV and the payload [18]. On the other hand, cable slackness would imply the load is in a free-fall condition, which is dangerous [19].*

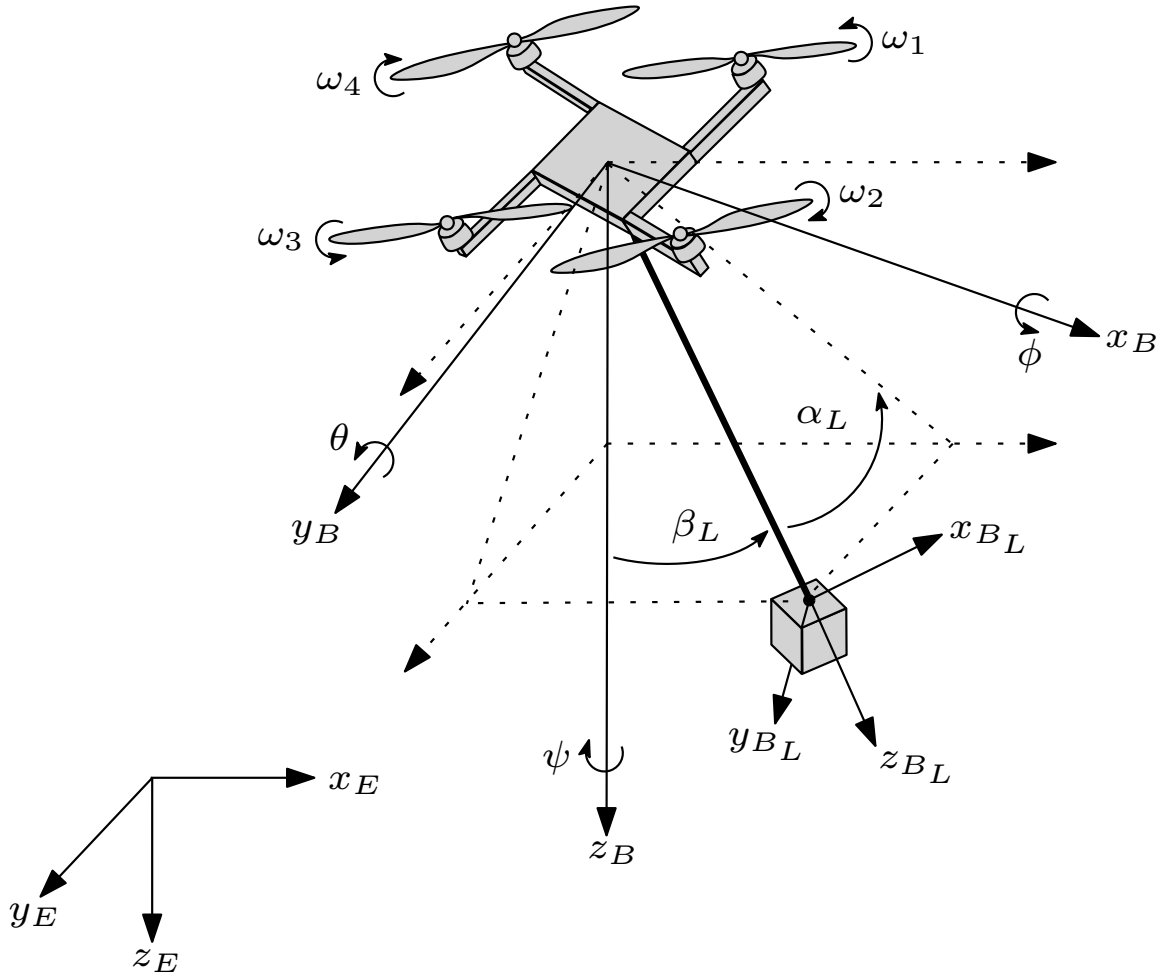

Fig. 1 Cargo drone, consisting of a quadrotor with a cable-suspended payload, after [15].

Based on Assumption 1, the equations are derived via Lagrangian computation. More specifically, the UAV translational dynamics result to be

$$\begin{cases} F_x = (m_Q + m_L)\ddot{x} - m_L l \mathrm{s}_{\alpha_L}\mathrm{s}_{\beta_L}\ddot{\alpha}_L + m_L l \mathrm{c}_{\alpha_L}\mathrm{c}_{\beta_L}\ddot{\beta}_L - 2m_L l \mathrm{c}_{\beta_L}\mathrm{s}_{\alpha_L}\dot{\alpha}_L\dot{\beta}_L - m_L l \mathrm{s}_{\beta_L}\mathrm{c}_{\alpha_L}(\dot{\alpha}_L^2 + \dot{\beta}_L^2), \\ F_y = (m_Q + m_L)\ddot{y} - m_L l \mathrm{c}_{\alpha_L}\ddot{\alpha}_L + m_L l \mathrm{s}_{\alpha_L}\dot{\alpha}_L^2, \\ F_z = (m_Q + m_L)(\ddot{z} - g) - m_L l \mathrm{s}_{\alpha_L}\mathrm{c}_{\beta_L}\ddot{\alpha}_L - m_L l \mathrm{c}_{\alpha_L}\mathrm{s}_{\beta_L}\ddot{\beta}_L + 2m_L l \mathrm{s}_{\beta_L}\mathrm{s}_{\alpha_L}\dot{\alpha}_L\dot{\beta}_L - m_L l \mathrm{c}_{\beta_L}\mathrm{c}_{\alpha_L}(\dot{\alpha}_L^2 + \dot{\beta}_L^2), \end{cases} \tag{1}$$

where $\mathrm{c}_{(\cdot)}$ and $\mathrm{s}_{(\cdot)}$ represent the $\cos(\cdot)$ and $\sin(\cdot)$ functions, respectively. This notation is adopted throughout the paper. Similarly, the UAV rotational dynamics are

$$\begin{cases} \tau_\phi = I_{Q_{xx}}\ddot{\phi} - I_{Q_{xx}}\mathrm{s}_\theta\ddot{\psi} - (I_{Q_{yy}} - I_{Q_{zz}})\mathrm{s}_\phi\mathrm{c}_\phi\mathrm{c}_\theta^2\dot{\psi}^2 + ((I_{Q_{yy}} - I_{Q_{zz}})(\mathrm{s}_\phi^2 - \mathrm{c}_\phi^2) - I_{Q_{xx}})\mathrm{c}_\theta\dot{\theta}\dot{\psi} \\ \quad + (I_{Q_{yy}} - I_{Q_{zz}})\mathrm{c}_\phi\mathrm{s}_\phi\dot{\theta}^2 + I_R\mathrm{c}_\phi\textstyle\sum\omega_i\dot{\theta} + I_R\mathrm{c}_\theta\mathrm{s}_\phi\sum\omega_i\dot{\psi}, \\ \tau_\theta = (I_{Q_{yy}}\mathrm{c}_\phi^2 + I_{Q_{zz}}\mathrm{s}_\phi^2)\ddot{\theta} + (I_{Q_{yy}} - I_{Q_{zz}})\mathrm{c}_\theta\mathrm{c}_\phi\mathrm{s}_\phi\ddot{\psi} + \mathrm{s}_\theta\mathrm{c}_\theta(-I_{Q_{xx}} + I_{Q_{yy}}\mathrm{s}_\phi^2 + I_{Q_{zz}}\mathrm{c}_\phi^2)\dot{\psi}^2 \\ \quad + ((I_{Q_{yy}} - I_{Q_{zz}})(\mathrm{c}_\phi^2 - \mathrm{s}_\phi^2) + I_{Q_{xx}})\mathrm{c}_\theta\dot{\phi}\dot{\psi} - 2(I_{Q_{yy}} - I_{Q_{zz}})\mathrm{c}_\phi\mathrm{s}_\phi\dot{\phi}\dot{\theta} - I_R\textstyle\sum\omega_i(\dot{\phi} - \mathrm{s}_\theta\dot{\psi}), \\ \tau_\psi = -I_{Q_{xx}}\mathrm{s}_\theta\ddot{\phi} + (I_{Q_{yy}} - I_{Q_{zz}})\mathrm{c}_\theta\mathrm{c}_\phi\mathrm{s}_\phi\ddot{\theta} + (I_{Q_{xx}}\mathrm{s}_\theta^2 + \mathrm{c}_\theta^2(I_{Q_{zz}}\mathrm{c}_\phi^2 + I_{Q_{yy}}\mathrm{s}_\phi^2))\ddot{\psi} \\ \quad - (I_{Q_{xx}} + (I_{Q_{yy}} - I_{Q_{zz}})(\mathrm{s}_\phi^2 - \mathrm{c}_\phi^2))\mathrm{c}_\theta\dot{\phi}\dot{\theta} - (I_{Q_{yy}} - I_{Q_{zz}})\mathrm{c}_\phi\mathrm{s}_\phi\mathrm{s}_\theta\dot{\theta}^2 \\ \quad + 2(I_{Q_{yy}} - I_{Q_{zz}})\mathrm{c}_\phi\mathrm{s}_\phi\mathrm{c}_\theta^2\dot{\phi}\dot{\psi} + 2(I_{Q_{xx}} - I_{Q_{yy}}\mathrm{s}_\phi^2 - I_{Q_{zz}}\mathrm{c}_\phi^2)\mathrm{c}_\theta\mathrm{s}_\theta\dot{\theta}\dot{\psi}. \end{cases} \tag{2}$$

Finally, the swing angles equations are

$$\begin{cases} g_{\alpha_L}\ddot{\alpha}_L = m_L l \mathrm{s}_{\alpha_L}\mathrm{s}_{\beta_L}\ddot{x} + m_L l \mathrm{s}_{\alpha_L}\mathrm{c}_{\beta_L}\ddot{z} + m_L l \mathrm{c}_{\alpha_L}\ddot{y} - m_L g l \mathrm{s}_{\alpha_L}\mathrm{c}_{\beta_L} - (m_L l^2 + I_{L_{yy}} - I_{L_{zz}})\mathrm{s}_{\alpha_L}\mathrm{c}_{\alpha_L}\dot{\beta}_L^2, \\ g_{\beta_L}\ddot{\beta}_L = -m_L l \mathrm{c}_{\alpha_L}\mathrm{c}_{\beta_L}\ddot{x} + m_L l \mathrm{s}_{\beta_L}\mathrm{c}_{\alpha_L}\ddot{z} - m_L g l \mathrm{s}_{\beta_L}\mathrm{c}_{\alpha_L} + 2(m_L l^2 + I_{L_{yy}} - I_{L_{zz}})\mathrm{s}_{\alpha_L}\mathrm{c}_{\alpha_L}\dot{\alpha}_L\dot{\beta}_L, \end{cases} \tag{3}$$

where $g_{\alpha_L} = m_L l^2 + I_{L_{xx}}$, and $g_{\beta_L} = m_L l^2 \mathrm{c}_{\alpha_L}^2 + I_{L_{yy}}\mathrm{c}_{\alpha_L}^2 + I_{L_{zz}}\mathrm{s}_{\alpha_L}^2$.

2.1 Simplified local model

The resulting dynamics are highly nonlinear and coupled. Hence, for control purposes, Eqs. (1) and (3) are further simplified, assuming that the load swing angles are small, and that higher order terms containing powers or products of α_L, β_L, $\dot{\alpha}_L$, $\dot{\beta}_L$ can be neglected. The simplified UAV translational dynamics and load swing angles dynamics are

$$\begin{cases} \ddot{x} \simeq \dfrac{1}{D_{\beta_L}}F_x - \dfrac{m_L^2 l^2}{(m_Q + m_L)g'_{\beta_L}D_{\beta_L}}\beta_L F_z, \\ \ddot{y} \simeq \dfrac{1}{D_{\alpha_L}}F_y + \dfrac{m_L^2 l^2}{(m_Q + m_L)D_{\alpha_L}g_{\alpha_L}}\alpha_L F_z, \\ \ddot{z} \simeq \dfrac{F_z}{m_Q + m_L} + g, \\ \ddot{\alpha}_L \simeq \dfrac{m_L l}{D_{\alpha_L}g_{\alpha_L}}\left(F_y + \alpha_L F_z\right), \\ \ddot{\beta}_L \simeq \dfrac{m_L l}{g'_{\beta_L}D_{\beta_L}}\left(-F_x + \beta_L F_z\right), \end{cases} \tag{4}$$

where $D_{\alpha_L} = (m_Q + m_L) - (m_L^2 l^2)/g_{\alpha_L}$, $g'_{\beta_L} = m_L l^2 + I_{L_{yy}}$, and $D_{\beta_L} = (m_Q + m_L) - (m_L^2 l^2)/g'_{\beta_L}$.

Problem 1 *Consider the simplified model of a quadrotor with a cable-suspended payload, given by Eqs.* (2) *and* (4)*. Assume that the vector* $\boldsymbol{q}$ *is available, together with the velocities and accelerations of both the UAV and the load. Given a desired smooth trajectory, design a controller that ensures asymptotic tracking of the reference trajectory, while driving the state trajectories of the load swing angles to a small region near the origin during cargo transportation.*

Remark 2 *Problem 1 is similar to the swing suppression problem of overhead cranes. In that context, the control objective is to move the load from a starting to a final point, while guaranteeing that the load oscillations remain close to zero [13].*

3 Methods

The control scheme proposed in this paper is shown in Fig. 2. It consists of the Super-Twisting sliding mode controllers with swing reduction, the control allocation, and the UAV-payload dynamics.

The structure of the controllers is hierarchical, and consists of four different blocks:

- Outer position control loop, which calculates the virtual control inputs F_x, F_y, and F_z;
- Decoupler, which computes the total thrust T and the roll and pitch references ϕ_{des} and θ_{des};
- Higher order sliding mode differentiators, which derive the desired angular rates and accelerations based on ϕ_{des} and θ_{des};
- Inner attitude control loop, which computes the torques τ_ϕ, τ_θ, τ_ψ.

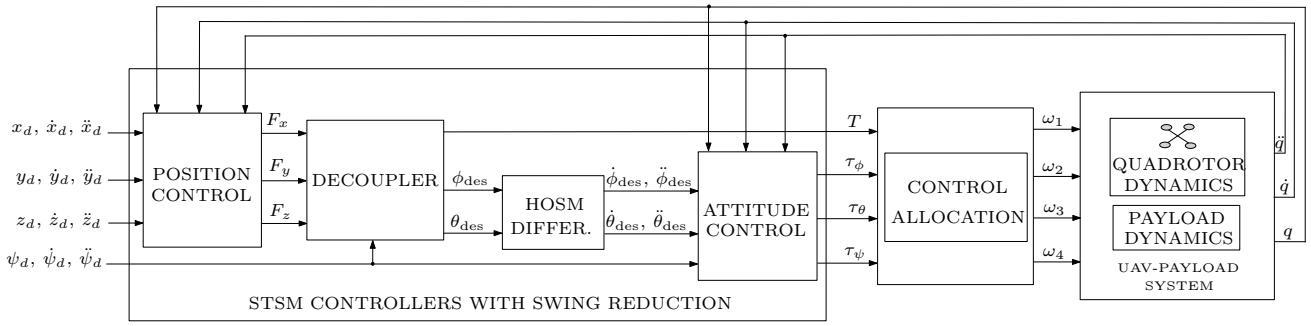

Fig. 2 Overall control scheme (after [15]).

From Eq. (4), it can be seen that $\ddot{x}$ is coupled with β_L, while $\ddot{y}$ is coupled with α_L. Inspired by the work of [13] and [14] on 3D overhead cranes, the sliding mode surfaces related to the x and the y channels are augmented with two terms that depend on the swing angles. A similar approach is proposed for cargo drones in [1], where the authors design first order sliding mode controllers aimed to suppress the load oscillations in the XZ plane. Differently from [1], we address the problem in three dimensional space and we propose second order sliding mode controllers based on the Super-Twisting Algorithm to reduce the chattering phenomenon.

3.1 Design of translational STSM controllers with swing reduction

In this subsection, the derivation of the STSM controller with swing reduction is carried out in detail to obtain F_x, but the same steps can be followed to derive F_y. Consider the $\ddot{x}$ and the $\ddot{\beta}_L$ dynamics given in Eq. (4). Let x_d be the reference value for the x position of the UAV. Defining $x_1 := x - x_d$, $x_2 := \dot{x} - \dot{x}_d$, $x_3 := \beta_L$, and $x_4 = \dot{\beta}_L$, we can write

$$\begin{cases} \dot{x}_1 = x_2, \\ \dot{x}_2 = b_{1x} F_x + g_{1x}(x), \\ \dot{x}_3 = x_4, \\ \dot{x}_4 = b_{2x} F_x + g_{2x}(x), \end{cases} \tag{5}$$

where the functions b_{1x}, $g_{1x}(x)$, b_{2x}, $g_{2x}(x)$ are obtained from Eq. (4). The sliding surface is defined as

$$s_x := c_{1x} x_1 + x_2 + c_{2x} x_3 + c_{3x} x_4. \tag{6}$$

Computing its first order derivative, we obtain

$$\dot{s}_x = c_{1x} x_2 + b_{1x} F_x + g_{1x}(x) + c_{2x} x_4 + c_{3x} b_{2x} F_x + c_{3x} g_{2x}(x). \tag{7}$$

The second order sliding mode controller based on the Super-Twisting Algorithm is formulated to drive both s_x and $\dot{s}_x$ to zero in finite time. The discontinuous signum function, which causes the chattering phenomenon in conventional sliding mode control, is incorporated in the higher derivatives of the sliding surface, hence resulting in a continuous control law with chattering mitigation. More specifically, the STSM control is given by two terms: the switching control, which drives the sliding surface to zero; the equivalent control, which drives the system along the sliding surface, once $s_x = 0$.

Starting from the equivalent term, imposing $\dot{s}_x = 0$, we get

$$F_{x_{\text{eq}}} = -\frac{c_{1x} x_2 + c_{2x} x_4 + g_{1x}(x) + c_{3x} g_{2x}(x)}{b_{1x} + c_{3x} b_{2x}}, \tag{8}$$

where the coefficients c_{1x}, c_{2x}, c_{3x} are calculated via Hurwitz analysis, inspired by [1] and [20]. In particular, when $s_x = \dot{s}_x = 0$, the system given by Eq. (5) can be linearized around the equilibrium point $[x_1, x_2, x_3, x_4]^T = [0, 0, 0, 0]^T$, yielding to the following reduced-order system

$$\begin{cases} \dot{x}_1 = -c_{1x}x_1 - c_{2x}x_3 - c_{3x}x_4, \\ \dot{x}_3 = x_4, \\ \dot{x}_4 = \dfrac{c_{1x}^2}{c_{3x}}x_1 + \left(\dfrac{c_{1x}c_{2x}}{c_{3x}} + \dfrac{m_L^2 l^2 F_z}{c_{3x}(m_Q + m_L)g'_{\beta_L} D_{\beta_L}}\right)x_3 + \left(c_{1x} - \dfrac{c_{2x}}{c_{3x}}\right)x_4. \end{cases} \tag{9}$$

Assuming $c_{3x} \neq 0$ and treating F_z as time-varying parameter, the coefficients of the sliding surface are calculated in order to guarantee that the eigenvalues of the state matrix of the linearized system belong to the left half-plane. In particular, setting the characteristic polynomial as $p(\lambda) = (\lambda + a)(\lambda + b)(\lambda + c)$, with $a, b, c > 0$, the following values are obtained

$$\begin{aligned} c_{1x} &= -abc\frac{(m_Q + m_L)g'_{\beta_L} D_{\beta_L}}{m_L^2 l^2 F_z}c_{3x}, \\ c_{2x} &= (a + b + c)c_{3x}, \\ c_{3x} &= -\frac{m_L^2 l^2 F_z}{(m_Q + m_L)g'_{\beta_L} D_{\beta_L}}\frac{1}{ab + bc + ac}. \end{aligned} \tag{10}$$

The switching term $F_{x_{\text{sw}}}$ is found imposing the reaching condition

$$\dot{s}_x = -k_{1x}|s_x|^{1/2}\,\text{sign}(s_x) - \int_0^t k_{2x}\,\text{sign}(s_x)d\tau, \tag{11}$$

where the gains k_{1x} and k_{2x} are positive. By setting $\dot{v}_x := -k_{2x}\,\text{sign}(s_x)$, $F_{x_{\text{sw}}}$ results to be

$$F_{x_{\text{sw}}} = \frac{1}{b_{1x} + c_{3x}b_{2x}}\left(-k_{1x}\,|s_x|^{1/2}\,\text{sign}\,(s_x) + v_x\right). \tag{12}$$

Finally, the overall virtual control input F_x is obtained via the combination of the equivalent term and the switching term.

Similarly, considering the y channel, F_y is given by the equivalent term

$$F_{y_{\text{eq}}} = -\frac{c_{1y}y_2 + c_{2y}y_4 + g_{1y}(y) + c_{3y}g_{2y}(y)}{b_{1y} + c_{3y}b_{2y}}, \tag{13}$$

and the switching term

$$F_{y_{\text{sw}}} = \frac{1}{b_{1y} + c_{3y}b_{2y}}\left(-k_{1y}|s_y|^{1/2}\,\text{sign}(s_y) + v_y\right). \tag{14}$$

Again, the gains k_{1y} and k_{2y} are selected to be positive, while c_{1y}, c_{2y}, c_{3y} are computed via linearization and Hurwitz analysis, resulting in the following expressions

$$\begin{aligned} c_{1y} &= abc\frac{(m_Q + m_L)g_{\alpha_L} D_{\alpha_L}}{m_L^2 l^2 F_z}c_{3y}, \\ c_{2y} &= (a + b + c)c_{3y}, \\ c_{3y} &= \frac{m_L^2 l^2 F_z}{(m_Q + m_L)g_{\alpha_L} D_{\alpha_L}}\frac{1}{ab + bc + ac}. \end{aligned} \tag{15}$$

3.2 Design of altitude and attitude STSM controllers

For what concerns the altitude and the attitude controllers, having no dependence on the load swing angles, the derivation follows the standard procedure employed with second order sliding mode techniques. Considering the z channel as an example, we can write $\ddot{z} = F_z/g_z + f_z$ from Eq. (4). Defining the tracking errors as $e_z := z - z_d$ and $\dot{e}_z := \dot{z} - \dot{z}_d$, the sliding surface is set to be $s_z := \lambda_z e_z + \dot{e}_z$, with $\lambda_z > 0$. Then, the virtual control input F_z is given by the combination of the equivalent term, found imposing $\dot{s}_z = 0$, and the switching term, calculated requiring the reaching condition $\dot{s}_z = -k_{1z}|s_z|^{1/2}\,\mathrm{sign}(s_z) - \int_0^t k_{2z}\,\mathrm{sign}(s_z)d\tau$. By setting $\dot{v}_z := -k_{2z}\,\mathrm{sign}(s_z)$, we obtain

$$F_z = g_z\left(\ddot{z}_d - f_z - \lambda_z\dot{e}_z - k_{1z}\,|s_z|^{1/2}\,\mathrm{sign}(s_z) + v_z\right). \tag{16}$$

The same reasoning is applied also to obtain the torques, yielding

$$\begin{aligned}
\tau_\phi &= g_\phi\left(\ddot{\phi}_{\mathrm{des}} - f_\phi - \lambda_\phi\dot{e}_\phi - k_{1\phi}|s_\phi|^{1/2}\,\mathrm{sign}(s_\phi) + v_\phi\right),\\
\tau_\theta &= g_\theta\left(\ddot{\theta}_{\mathrm{des}} - f_\theta - \lambda_\theta\dot{e}_\theta - k_{1\theta}\,|s_\theta|^{1/2}\,\mathrm{sign}(s_\theta) + v_\theta\right),\\
\tau_\psi &= g_\psi\left(\ddot{\psi}_d - f_\psi - \lambda_\psi\dot{e}_\psi - k_{1\psi}|s_\psi|^{1/2}\,\mathrm{sign}(s_\psi) + v_\psi\right).
\end{aligned} \tag{17}$$

Remark 3 *In order to compute the torques τ_ϕ and τ_θ, the desired angular velocities $\dot{\phi}_{\mathrm{des}}$, $\dot{\theta}_{\mathrm{des}}$ and the desired angular accelerations $\ddot{\phi}_{\mathrm{des}}$, $\ddot{\theta}_{\mathrm{des}}$ are needed. Their derivation is carried out from ϕ_{des}, θ_{des}, exploiting the higher order sliding mode (HOSM) differentiator [21]*

$$\begin{cases}
\dot{z}_0 = v_0, \quad v_0 = -3L^{1/3}\,|z_0 - f|^{2/3}\,\mathrm{sign}\,(z_0 - f) + z_1,\\
\dot{z}_1 = v_1, \quad v_1 = -1.5L^{1/2}\,|z_1 - v_0|^{1/2}\,\mathrm{sign}\,(z_1 - v_0) + z_2,\\
\dot{z}_2 = -1.1L\,\mathrm{sign}\,(z_2 - v_1)\,,
\end{cases} \tag{18}$$

where f is the signal to be differentiated, z_1 and z_2 represent its first and second derivatives respectively, and L denotes the gain of the HOSM differentiator.

3.3 Stability analysis

The stability analysis of the proposed STSM controllers is shown below considering the x channel, but the procedure can be extended and applied for the other controllers as well. Substituting $F_{x_{\mathrm{eq}}}$ and $F_{x_{\mathrm{sw}}}$ into Eq. (7), the dynamics along the sliding surface are described by the following system

$$\begin{cases}
\dot{s}_x = -k_{1x}|s_x|^{1/2}\,\mathrm{sign}(s_x) + v_x,\\
\dot{v}_x = -k_{2x}\,\mathrm{sign}(s_x).
\end{cases} \tag{19}$$

At this point, it is possible to prove that if $k_{1x},\ k_{2x} > 0$, then s_x and v_x converge to zero in finite time. As done in [22], let us define the Lyapunov function

$$V_x\,(s_x, v_x) = 2k_{2x}\,|s_x| + \frac{1}{2}v_x^2 + \frac{1}{2}\left(k_{1x}\,|s_x|^{1/2}\,\mathrm{sign}\,(s_x) - v_x\right)^2. \tag{20}$$

If we set $\zeta_x^T = \left[|s_x|^{1/2}\,\mathrm{sign}(s_x),\ v_x\right]^T$, V_x can be rewritten as a quadratic form $V_x = \zeta_x^T P_x \zeta_x$, where the matrix P_x is given by

$$P_x = \frac{1}{2}\begin{bmatrix} 4k_{2x} + k_{1x}^2 & -k_{1x} \\ -k_{1x} & 2 \end{bmatrix}. \tag{21}$$

Hence, it results that V_x is positive definite and radially unbounded if $k_{2x} > 0$. Computing the time derivative, we get

$$\dot{V}_x = -\frac{1}{|s_x|^{1/2}}\zeta_x^\top Q_x \zeta_x, \tag{22}$$

with

$$Q_x = \frac{k_{1x}}{2}\begin{bmatrix} 2k_{2x} + k_{1x}^2 & -k_{1x} \\ -k_{1x} & 1 \end{bmatrix}. \tag{23}$$

Consequently, $\dot{V}_x < 0$ if $Q_x > 0$, giving k_{1x}, $k_{2x} > 0$. Using the fact that $\lambda_{\min}\{P_x\}\,\|\zeta_x\|_2^2 \leqslant V_x \leqslant \lambda_{\max}\{P_x\}\,\|\zeta_x\|_2^2$, where $\lambda_{\min}\{P_x\}$ and $\lambda_{\max}\{P_x\}$ denote the minimum and maximum eigenvalue of P_x, and having $\dot{V}_x \leq -1/|s_x|^{1/2}\lambda_{\min}\{Q_x\}\,\|\zeta_x\|_2^2$, after some mathematical manipulation it results that

$$\dot{V}_x \leq -\frac{\lambda_{\min}\{Q_x\}\,\lambda_{\min}\{P_x\}}{\lambda_{\max}\{P_x\}} V_x^{1/2}. \tag{24}$$

Integrating both sides of the inequality, we finally obtain that V_x converges to zero in finite time T_x, where

$$T_x = \frac{2V_x^{1/2}\left(s_{x_0}, v_{x_0}\right)}{\gamma_x}, \tag{25}$$

with s_{x_0} and v_{x_0} being the initial states, and $\gamma_x = \lambda_{\min}\{Q_x\}\,\lambda_{\min}\{P_x\}/\lambda_{\max}\{P_x\}$.

4 Simulations

Simulations performed in Matlab and Simulink are shown and discussed in this section. The parameters of the cargo drone in Table 2 are taken from [15], and correspond to a small-scale quadrotor carrying a small payload.

Table 2 Cargo drone parameters.

Parameter	Value	Parameter	Value
g	9.81 m/s^2	$I_{Q_{xx}} = I_{Q_{yy}}$	13.2×10^{-3} kg × m^2
m_Q	1.56 kg	$I_{Q_{zz}}$	2.51×10^{-2} kg × m^2
r_Q	0.225 m	m_L	0.2 kg
c_T	1.228×10^{-5} N/(rad/s)^2	r_L	0.09 m
c_M	5×10^{-7} N/(rad/s)^2	$I_{L_{xx}} = I_{L_{yy}} = I_{L_{zz}}$	3.9×10^{-5} kg × m^2
I_R	1×10^{-6} kg × m^2	l	1.5 m

The coefficients of the sliding surfaces and STSM controllers with swing reduction are reported in Table 3. The initial UAV position and orientation and the initial load swing angles are embedded in the vector $\boldsymbol{q}_0 = [5,\ 0,\ -1.5,\ 0,\ 0,\ 0,\ 0,\ 0]^T$. In this way, the quadrotor is hovering at 1.5 meters from the ground, the cable results to be taut, and the load is not yet in the air.

Table 3 Coefficients of sliding surfaces and STSM controllers.

Parameter	Value	Parameter	Value	Parameter	Value
a	8	b	6	c	7
k_{1x}	0.03	k_{2x}	0.01	k_{1y}	0.04
k_{2y}	0.02	λ_z	5	k_{1z}	3
k_{2z}	0.25	$\lambda_\phi = \lambda_\theta = \lambda_\psi$	5	$k_{1\phi} = k_{1\theta}$	0.1
$k_{2\phi} = k_{2\theta}$	0.02	$k_{1\psi}$	3	$k_{2\psi}$	0.2

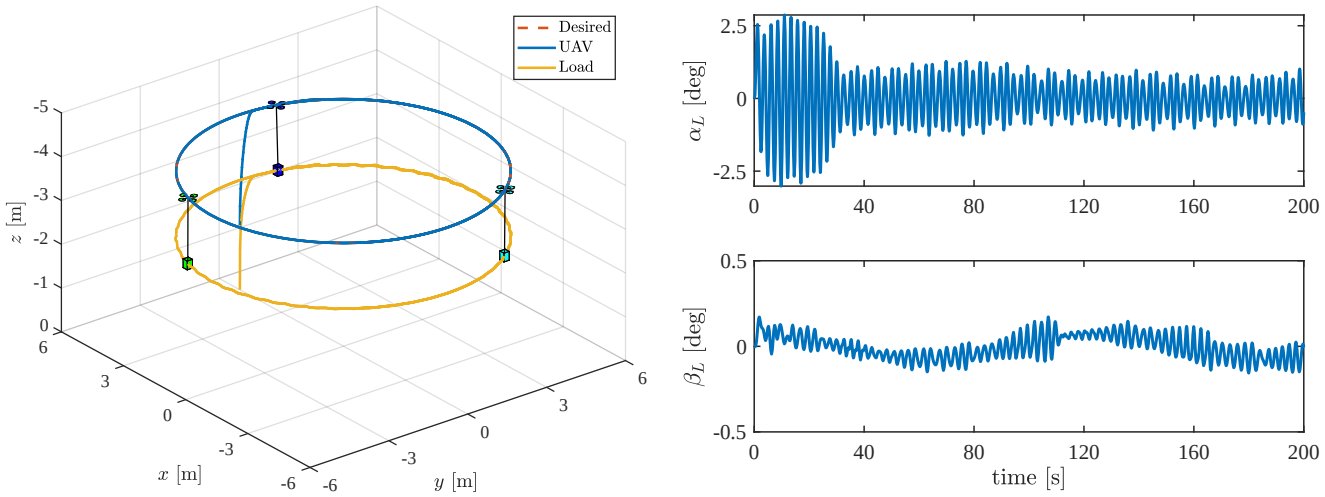

(a) UAV and load trajectories in the 3D space. **(b) Evolution of the load swing angles.**

Fig. 3 Case 1: 3D trajectories and load swing angles achieved using the proposed STSM controllers with swing reduction.

Two different scenarios are simulated: in the first case, the vehicle is required to follow a circular trajectory, after reaching a constant altitude, while in the second case the cargo drone performs a helical path. In both scenarios, the proposed controllers with active swing reduction are compared with the standard STSM controllers from [15], to demonstrate both the effective reduction of the load swing angles and the mitigation of the chattering phenomenon.

Case 1: In the first set of simulations, the reference trajectory is a circle given by $x_d = 5\cos(0.05t)$ m, $y_d = 5\sin(0.05t)$ m, $z_d = -4$ m, and $\psi_d = 0°$.

The resulting trajectories followed by the aerial vehicle and the cable-suspended load are shown in Fig. 3a. Different colors are used to represent the UAV-payload system at three time instants: $t = 5$ s (blue), $t = 50$ s (light blue), and $t = 100$ s (green). As emerges from the figure, the desired UAV trajectory is tracked with the designed STSM controllers. The circular paths of both the quadrotor and the load are smooth, even if the cable-suspended payload is characterized by a swinging behavior. On the other hand, the proposed control scheme effectively reduces the load oscillations, as shown in Fig. 3b. Indeed, α_L does not exceed a magnitude of 2.5°, while β_L is confined to an even smaller interval, qualitatively [-0.25, 0.25] degrees.

The position and the yaw angle of the quadrotor are depicted in Fig. 4a together with their reference values, while the convergence of the position tracking errors to zero can be verified in Fig. 4b. The

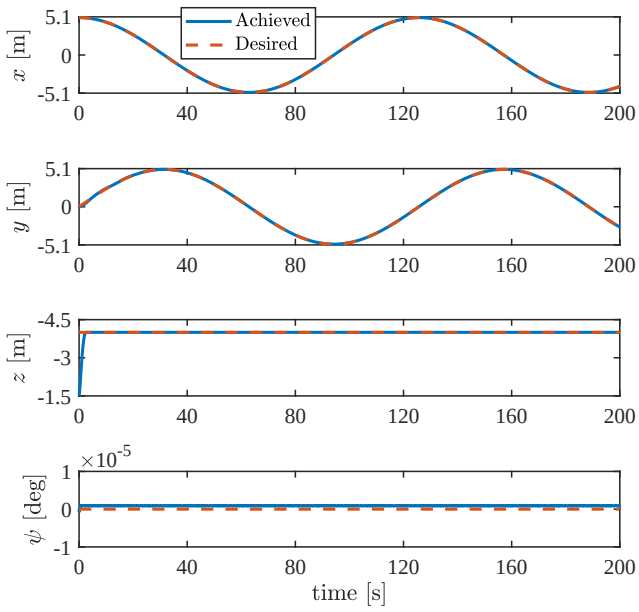

(a) Achieved and desired x, y, z, ψ.

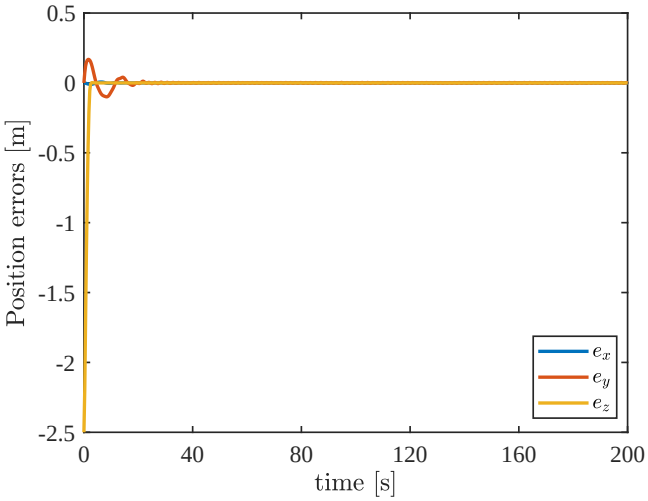

(b) Convergence of UAV position tracking errors.

Fig. 4 Case 1: Tracking performance of the proposed STSM controllers with swing reduction.

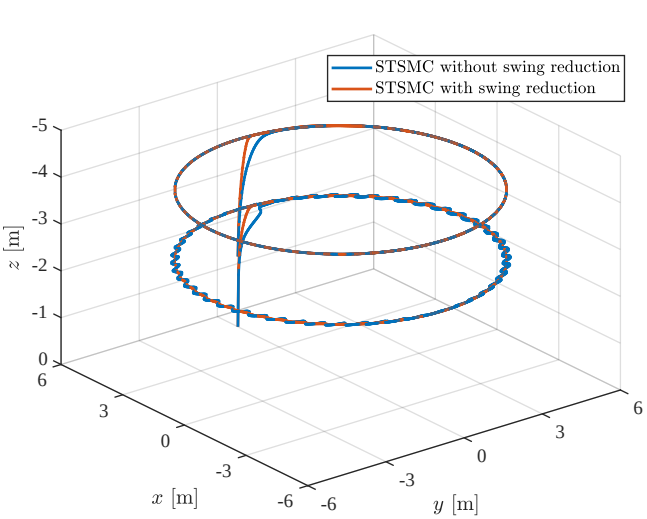

(a) Comparison of 3D trajectories.

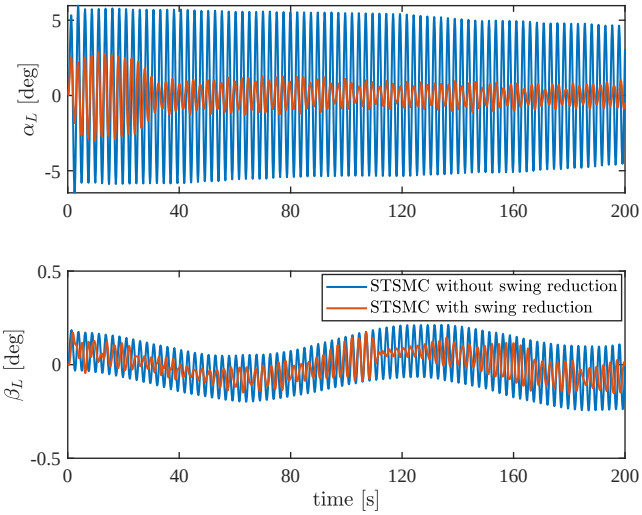

(b) Comparison of load swing angles.

Fig. 5 Case 1: Comparison between STSM controllers without and with swing reduction.

proposed second order sliding mode controllers based on the Super-Twisting Algorithm ensure that the reference values x_d, y_d, z_d, and ψ_d are followed by the UAV after less than 5 seconds.

To further highlight the capabilities of the proposed control scheme, we compare the STSM controllers with swing reduction to the standard STSM controllers proposed in [15]. The 3D trajectories and the load oscillations under the two different controllers are presented and compared in Fig. 5. While the UAV follows qualitatively the same trajectory under both control strategies, smaller load oscillations are observed when active swing reduction is employed. More specifically, the controllers proposed in this work permit to suppress the load swing angles by more than 50% when compared to STSMCs without active swing reduction. In addition to dampen the load oscillations, the controllers permit to further mitigate chattering in the control inputs, as highlighted in Fig. 6.

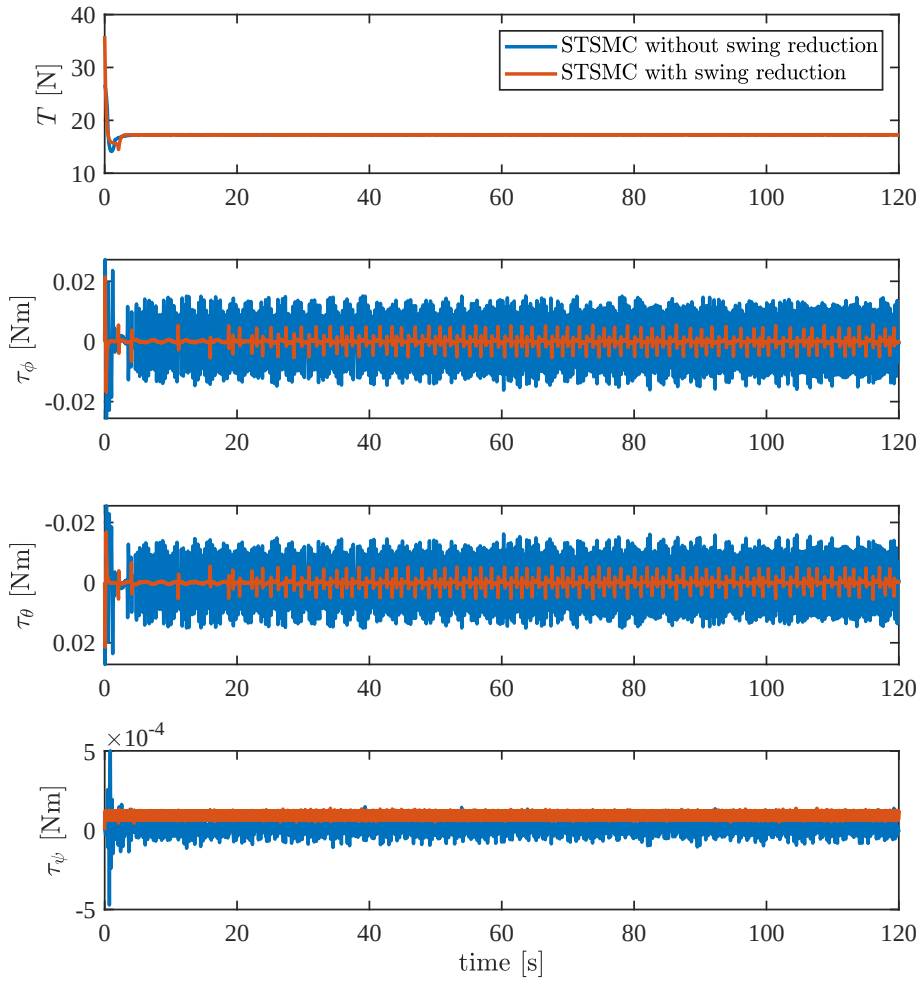

Fig. 6 Case 1: Comparison between control inputs of STSM controllers without and with swing reduction.

Case 2: In the second set of simulations, the reference trajectory is a helix given by $x_d = 5\cos(0.05t)$ m, $y_d = 5\sin(0.05t)$ m, $z_d = -0.2t$ m, and $\psi_d = 0°$. In this way, the cargo quadrotor is required to track a spiral-shaped trajectory, ascending with a constant velocity of 0.2 m/s.

The proposed STSM controllers with swing reduction permit to achieve satisfactory results, as observed in Fig. 7. Also in this scenario, the inclusion of the swing angles dynamics in the sliding surfaces results in higher reduction of the load oscillations and chattering mitigation, as highlighted in Fig. 8.

5 Conclusions

In this paper, we present a set of second order sliding mode controllers based on the Super-Twisting Algorithm to drive a cargo drone along a predefined trajectory, while reducing the load oscillations. First, the model of the UAV-payload system is derived using the Lagrangian formulation. Then, the translational equations of motion are decoupled and simplified, employing the small angle assumption. In order to dampen the swinging behavior of the cable-suspended load, the sliding surfaces of the translational subsystem are defined combining both the tracking errors and the swing angle dynamics. The coefficients are computed via linearization and Hurwitz analysis to ensure the stability of the reduced-order dynamics during the sliding phase. For the altitude and attitude control, the coefficients of the STSM controllers are obtained through Lyapunov analysis, ensuring that the sliding surfaces converge to zero in finite time. Simulations carried out in Matlab and Simulink show that, under the designed

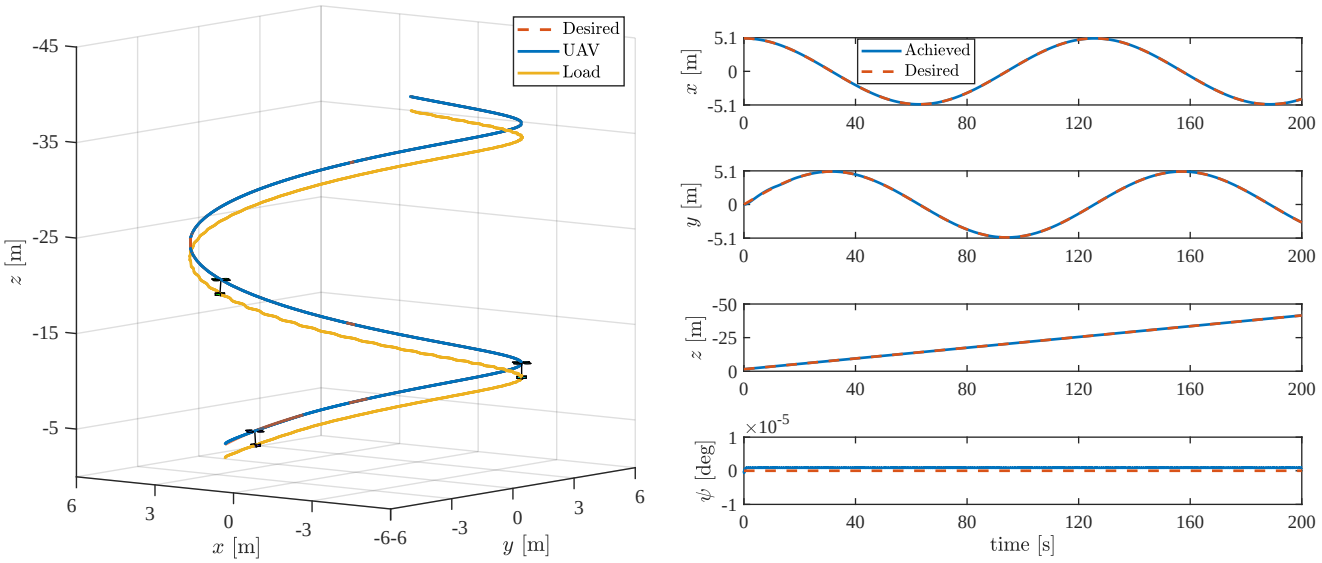

(a) UAV and load trajectories in the 3D space. **(b) Achieved and desired x, y, z, ψ.**

Fig. 7 Case 2: 3D trajectories and tracking performance achieved using the proposed STSM controllers with swing reduction.

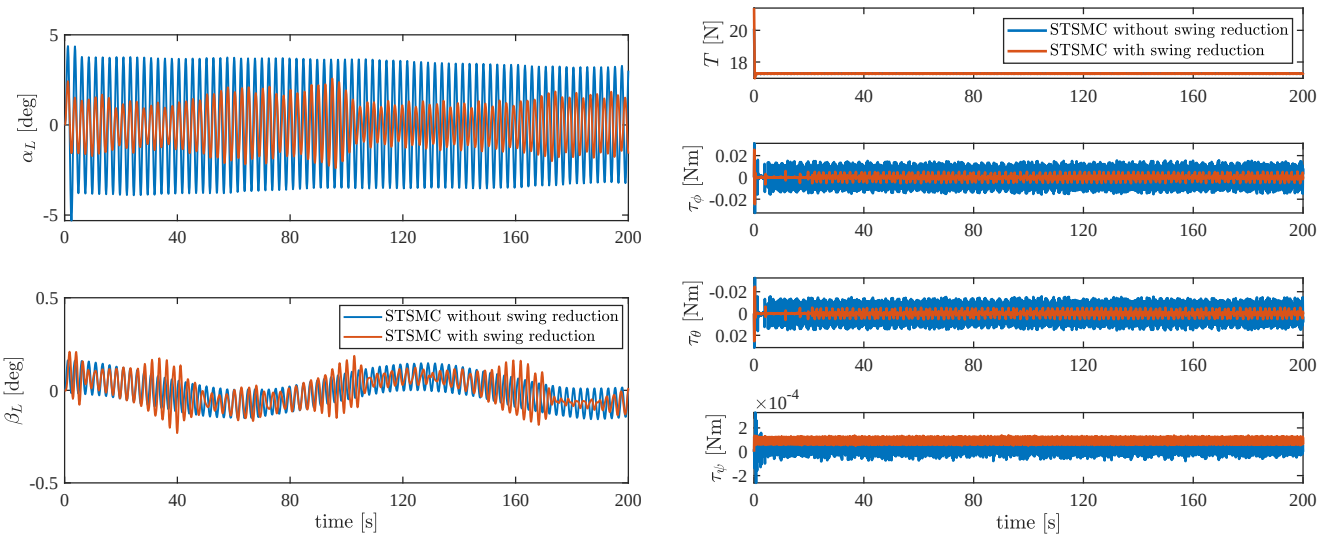

(a) Comparison of load swing angles. **(b) Comparison of control inputs.**

Fig. 8 Case 2: Comparison between STSM controllers without and with swing reduction.

controllers, the load swing angles are confined between [-2.5, 2.5] degrees. Moreover, the oscillations are reduced by more than 50% when compared to standard STSMCs without active swing reduction. In the future, we plan to test the proposed controllers on real vehicles, integrating strategies for the measurement of the swing angles.

Acknowledgments

This project is co-funded by the European Union – Next Generation EU - under the National Recovery and Resilience Plan (NRRP), Mission 4 Component 1 Investment 4.1 - Decree No. 118 (2nd March 2023) of Italian Ministry of University and Research - Concession Decree No. 2333 (22nd December 2023) of the Italian Ministry of University and Research, Project code D93C23000450005, within the Italian National PhD Program in Autonomous Systems (DAuSy).

Declaration of Use of Artificial Intelligence

Artificial intelligence was not used in the work presented.

References

[1] Tom Kusznir and Jaroslaw Smoczek. Sliding mode-based control of a UAV quadrotor for suppressing the cable-suspended payload vibration. *Journal of Control Science and Engineering*, 2020. doi: 10.1155/2020/5058039.

[2] Daniel K. D. Villa, Alexandre S. Brandão, and Mário Sarcinelli-Filho. A survey on load transportation using multirotor UAVs. *Journal of Intelligent & Robotic Systems*, 98(2):267–296, 2020. doi: 10.1007/s10846-019-01088-w.

[3] Ameya R. Godbole and Kamesh Subbarao. Nonlinear control of unmanned aerial vehicles with cable suspended payloads. *Aerospace Science and Technology*, 93:105299, 2019. doi: 10.1016/j.ast.2019.07.032.

[4] Sangheon Lee and Hungsun Son. Antisway control of a multirotor with cable-suspended payload. *IEEE Transactions on Control Systems Technology*, 29(6):2630–2638, 2021. doi: 10.1109/TCST.2020.3035004.

[5] Julian Estevez, Gorka Garate, Jose Manuel Lopez-Guede, and Mikel Larrea. Review of aerial transportation of suspended-cable payloads with quadrotors. *Drones*, 8(2):35, 2024. doi: 10.3390/drones8020035.

[6] S. Sadr, S. Ali A. Moosavian, and P. Zarafshan. Dynamics modeling and control of a quadrotor with swing load. *Journal of Robotics*, 2014:1–12, 2014. doi: 10.1155/2014/265897.

[7] M. Eusebia Guerrero-Sánchez, D. Alberto Mercado-Ravell, Rogelio Lozano, and C. Daniel García-Beltrán. Swing-attenuation for a quadrotor transporting a cable-suspended payload. *ISA Transactions*, 68:433–449, 2017. doi: 10.1016/j.isatra.2017.01.027.

[8] Ziyou Zhang, Dong Zhang, Dezhi Kong, and Yanqian Wang. Real-time local obstacle avoidance and trajectory tracking control of quadrotor UAVs with suspended payload in complex environments. *IEEE Access*, 11:144017–144029, 2023. doi: 10.1109/ACCESS.2023.3344578.

[9] Sen Yang, Bin Xian, Jiaming Cai, and Guangyi Wang. Finite-time convergence control for a quadrotor unmanned aerial vehicle with a slung load. *IEEE Transactions on Industrial Informatics*, 20(1):605–614, 2024. doi: 10.1109/TII.2023.3268762.

[10] Renan S Geronel and Douglas D Bueno. Adaptive sliding mode control for vibration reduction on UAV carrying a payload. *Journal of Vibration and Control*, 31(5):721–737, 2025. doi: 10.1177/10775463241231845.

[11] Xu Zhou, Rui Liu, Jiucai Zhang, and Xiaoli Zhang. Stabilization of a quadrotor with uncertain suspended load using sliding mode control. In *Volume 5A: 40th Mechanisms and Robotics Conference*, Charlotte, North Carolina, USA, 2016. American Society of Mechanical Engineers. doi: 10.1115/DETC2016-60060.

[12] Farhad A. Goodarzi, Daewon Lee, and Taeyoung Lee. Geometric control of a quadrotor UAV transporting a payload connected via flexible cable. *International Journal of Control, Automation and Systems*, 13(6):1486–1498, 2015. doi: 10.1007/s12555-014-0304-0.

[13] Alessandro Pisano, Stefano Scodina, and Elio Usai. Load swing suppression in the 3-dimensional overhead crane via second-order sliding-modes. In *2010 11th International Workshop on Variable Structure Systems (VSS)*, pages 452–457. IEEE, 2010. doi: 10.1109/VSS.2010.5545138.

[14] Carlos Vázquez, Joaquin Collado, and Leonid Fridman. Super twisting control of a parametrically excited overhead crane. *Journal of the Franklin Institute*, 351(4):2283–2298, 2014. doi: 10.1016/j.jfranklin.2013.02.011.

[15] Sara Gomiero and Karl Von Ellenrieder. Modified super-twisting sliding mode control for trajectory tracking of a cargo quadrotor. In *2025 IEEE 21st International Conference on Automation Science and Engineering (CASE)*, pages 2116–2123, Los Angeles, CA, USA, 2025. doi: 10.1109/CASE58245.2025.11164044.

[16] Sara Gomiero and Karl Von Ellenrieder. Chattering-free sliding mode control for position and attitude tracking of a quadrotor with a cable-suspended load. In *2024 IEEE 20th International Conference on Automation Science and Engineering (CASE)*, pages 2031–2038. IEEE, 2024. doi: 10.1109/CASE59546.2024.10711727.

[17] Kristian Klausen, Thor I. Fossen, and Tor Arne Johansen. Nonlinear control of a multirotor UAV with suspended load. In *2015 International Conference on Unmanned Aircraft Systems (ICUAS)*, pages 176–184, Denver, CO, USA, June 2015. doi: 10.1109/ICUAS.2015.7152289.

[18] Longchao Ru, Jiale Liu, Binqi Chen, Dengnuo Chen, and Zeyin Fan. Adaptive sliding mode control of quadrotor system with elastic load connection of unknown mass. *Drones*, 8(12):708, 2024. doi: 10.3390/drones8120708.

[19] Jiacheng Liang, Yaonan Wang, Hang Zhong, Yanjie Chen, Hongwen Li, Hean Hua, and Wei Wang. Robust adaptive tracking control for aerial transporting a cable-suspended payload using backstepping sliding mode techniques. *IEEE Transactions on Automation Science and Engineering*, 22:4490–4500, 2025. doi: 10.1109/TASE.2024.3355225.

[20] Sara Gomiero and Karl D. Von Ellenrieder. Modeling and sliding mode control of a heavy-lift quadrotor with a cable-suspended payload under wind disturbances. *IEEE Transactions on Automation Science and Engineering*, 2025. doi: 10.1109/TASE.2025.3612189.

[21] Arie Levant. Higher-order sliding modes, differentiation and output-feedback control. *International Journal of Control*, 76(9):924–941, 2003. doi: 10.1080/0020717031000099029.

[22] Jaime A. Moreno and Marisol Osorio. A lyapunov approach to second-order sliding mode controllers and observers. In *2008 47th IEEE Conference on Decision and Control*, pages 2856–2861. IEEE, 2008. doi: 10.1109/CDC.2008.4739356.